Supplement of Atmos. Chem. Phys., 21, 8273–8292, 2021
https://doi.org/10.5194/acp-21-8273-2021-supplement

Supplement of

Source apportionment of carbonaceous aerosols in Beijing with radiocarbon and organic tracers: insight into the differences between urban and rural sites

Siqi Hou et al.

Correspondence to: Roy M. Harrison (r.m.harrison@bham.ac.uk) and Zongbo Shi (z.shi@bham.ac.uk)

Influence from Regional Transport

During the wintertime, air masses transported to Beijing were mainly from Inner Mongolia, Shanxi and Hebei, where the open burning activities were associated with maize straw (Zhang et al., 2019). During summer, air masses from Shandong, Hebei, Liaoning and Tianjin may bring particles from burning of wheat straw. However, for Inner Mongolia and Shanxi, little wheat is grown in these areas (Zhang et al., 2019; Zhou et al., 2017) and the influence of wheat straw burning is less important. The fire spot intensity, transport direction and sources of biomass burning are summarized in Table S1.

The high fire spot intensity indicates a strong likelihood of regional transport. However, the concentrations of LG would decrease with atmospheric transport by aging, varying with environmental conditions (Bhattarai et al., 2019), which can be used to infer the influence from regional transport and local emissions. For example, with similar $PM_{2.5}$ concentrations, the LG concentration on 26 November was much lower than that on 3 December. Considering the different intensity of fire spots between the two days, LG on 26 November may arise more from regional transport instead of local emissions. Moreover, the LG concentration on 2 December was similar to that on 3 December, but the $PM_{2.5}$ concentration was much lower. This implies a contribution from local sources in addition to regional transport on 2 December.

Detailed Method of Ratio Selection and Sensitivity Test for Quantification of Biomass Burning

As mentioned in the main text, softwood, maize straw and wheat straw are the main types of biomass fuels used within the region. The ratios of EC/OC and OC/LG from softwood, maize straw and wheat straw are summarized in Table S2.

As the fraction of LG from wood burning (f_{wood}) and straw burning (f_{straw}= 1- f_{wood}) are each in the range of 0 to 1, only those matching this limitation were selected when calculating OC_{bb}. Emission factors of LG from various biofuels showed that the LG emission from wheat straw was hundreds of times higher than from the values for wood combustion, while the emission factors are similar between maize and wood (Yan et al., 2018). It means that although the consumption of wheat straw may be less than that of wood, LG emission from wheat straw may exceed that from wood, and f_{wood} may be quite small in summer. Besides, the sum of calculated OC_{straw} and OC_{wood} should not exceed the measured OC_{nf} concentrations, which is another limitation for selecting EC/OC and OC/LG ratios. Hence, ratios of softwood from No. 25 to No. 37 in Table S3 with ratios of maize (No. 48 in Table S3) were used for the wintertime, and No. 30-37 with No. 42-45, 50 from softwood and wheat straw respectively were used in the summertime estimation of f_{wood}

OC_{bb} from each type of softwood and crop straw combination can be estimated once f_{wood} was confirmed, and then these were averaged. To further assess the sensitivity of the calculated OC_{bb} results to the different ratio sets, concentrations of OC_{bb} for each set of ratios have been plotted vs. the averaged values (Fig. S4). Compared to OC_{wood}, concentrations of OC_{straw} show a small spread, and are in narrow ranges. It means the OC_{straw} are less affected by the varying ratios, as the range of ratios is smaller. According to Fig. S4, there are large uncertainties attached to the estimated values of OC_{wood}, but not OC_{straw}. The uncertainties from OC_{bb} can further affect the estimation of OC from cooking, but have no influence on estimates of SOC, which are determined from the $(OC/EC)_{min}$ ratios. The accuracy of this extended Gelencsér method would increase if the softwood types and ratios were confirmed.

The concentrations and contributions of OC_{bb} are shown in Fig. S5. The uncertainties of OC_{bb} are calculated considering the uncertainties of EC_{nf} and LG:

$$u(OC_{bb})=\sqrt{\sum\left[\left(\frac{a-b}{ac-bd}\right)^2 u(EC_{nf})^2+\left(\frac{abc-abd}{ac-bd}\right)^2 u(LG)^2\right]}$$

where $a=(OC/LG)_{wood}$, $b=(OC/LG)_{straw}$, $c=(EC/OC)_{wood}$, and $d=(EC/OC)_{straw}$.

The average uncertainty of the LG concentration is 15%. The uncertainty of EC_{nf} is calculated by combining all the uncertainties from EC concentrations, f_{NF}, f_M and f_{ref}. The average uncertainty of OC_{bb} is 48.6%.

Determination of $(OC/EC)_{f,\,min}$ and $(OC/EC)_{nf,\,min}$ ratios and the estimation of POC_f and POC_{nf}

OC/EC ratios are seen as an indicator of aerosol emission sources to estimate the POC and SOC concentrations. ^{14}C analysis can provide OC to EC ratios from fossil and non-fossil sources ($(OC/EC)_f$ and $(OC/EC)_{nf}$). Herein, we use the lowest $(OC/EC)_f$ and $(OC/EC)_{nf}$ ratios ($(OC/EC)_{f,\,min}$ and $(OC/EC)_{nf,\,min}$, respectively) to represent primary OC/EC emission ratio to calculate primary fossil-derived and non-fossil-derived OC (POC_f and POC_{nf}) respectively. To avoid the overestimation of POC_f and POC_{nf} from the measured $(OC/EC)_{f,\,min}$ and $(OC/EC)_{nf,\,min}$ due to the limited samples for ^{14}C analysis in this study, it is necessary to evaluate $(OC/EC)_{nf,\,min}$ and $(OC/EC)_{f,\,min}$ ratios for the whole sampling period.

The relationship of $(OC/EC)_{nf}$ and $(OC/EC)_f$ with OC/EC can be described as follow,

$$\left(\frac{OC}{EC}\right)_{nf} = \frac{f_{NF,OC}}{f_{NF,EC}} \times \frac{OC}{EC}$$

$$\left(\frac{OC}{EC}\right)_{f} = \left(\frac{1-f_{NF,OC}}{1-f_{NF,EC}}\right) \times \frac{OC}{EC}$$

where $f_{NF,\,OC}$ and $f_{NF,\,EC}$ are the non-fossil fractions of OC and EC, $(1-f_{NF,\,OC})$ and $(1-f_{NF,\,EC})$ are the fossil fractions of OC and EC.

Ratios of $(OC/EC)_{nf}$ are determined by $\frac{f_{NF,OC}}{f_{NF,EC}}$ and OC/EC, therefore $(OC/EC)_{nf,\,min}$ can be roughly quantified by multiplying the lowest 5% OC/EC ratios with the lowest two $\frac{f_{NF,OC}}{f_{NF,EC}}$ ratios. Similarly, $(OC/EC)_{f,\,min}$ can be estimated by multiplying the lowest 5% OC/EC ratios with the lowest two $\left(\frac{1-f_{NF,OC}}{1-f_{NF,EC}}\right)$ ratios. The estimated $(OC/EC)_{nf,\,min}$ and $(OC/EC)_{f,\,min}$ ratios for IAP and PG sites in winter and summer sampling period were listed in Table S4. The estimated $(OC/EC)_{nf, min}$ and $(OC/EC)_{f, min}$ ratios are within the values of OC/EC emission ratios from coal combustion (1.5-15), traffic emission (0.69-1.01), and biomass burning (3-7) (Ni et al., 2018). Higher $(OC/EC)_{f, min}$ ratios in winter are consistent with the fact of elevated coal combustion compared to traffic emissions. It indicated the evaluation of $(OC/EC)_{nf, min}$ and $(OC/EC)_{f, min}$ ratios are reasonable.

Discussion of OC from cooking and OC from other potential non-fossil sources.

Cholesterol is an organic marker which is used to calculate OC from cooking in previous study. Thus, calculations of OC_{ck-ch} by cholesterol concentrations multiplying OC to cholesterol ratios (Zhao et al., 2015; Wu et al., 2021) were conducted to compare the EG method result (OC_{ck-EG}). The concentrations of cholesterol in 25 selected samples with the corresponding OC from cooking (OC_{ck-ch}) are summarized in Table S5. The methodology of cholesterol determination is described in Xu et. al (2020). The average concentrations of OC_{ck-ch} are 2.08±1.16 μg m^{-3} and 1.64±1.01 μg m^{-3} at IAP in winter and summer, 2.65 ±1.06 μg m^{-3} and 0.92±0.43 μg m^{-3} at PG in winter and summer. The OC_{ck-ch} concentrations are 1.8 times higher than the OC_{ck} from the EG method (OC_{ck-EG}) on average at IAP, and will result in the values of OC_{bb} + OC_{ck-ch} being much higher than POC_{nf}. It is suggested that the OC_{ck-ch} may contain some secondary OC. At PG, however, concentrations of OC_{ck-ch} are only half of OC_{ck-EG}. the OC_{ck-EG} is calculated by subtracting OC_{bb} from POC_{nf} assuming it arises mainly from cooking. Here, the much higher OC_{ck-EG} than OC_{ck-ch} at PG suggest that the OC_{ck-EG} may include other primary sources.

Comparisons of OC_{ck-ch} with OC_{ck-EG}, OC_{ck} from the CMB model and cooking OC from AMS/ACSM-PMF are shown in Figure 1(Figure S8 in SI). The concentrations of OC_{ck-ch} are not well correlated with CMB results or AMS/ACSM-PMF results. But the OC_{ck-ch} values are 6.5 times higher than CMB results on average, and 0.91 times the AMS/ACSM-PMF results. It is possible that the OC_{ck-ch} may contain secondary OC.

OC_{ck-ch} at PG is half of OC_{ck-EG}. We found the differences between OC_{ck-EG} and OC_{ck-ch} (OC_{onf}) at PG are positively correlated with crustal elements, Si, Al, Fe and Ti (shown in Figure 2, Figure S9 in SI). This indicates that the OC_{ck-EG} may include OC fractions from primary sources like dust. The filters collected during the APHH-campaign have been subject to elemental analysis with XRF and ICP-MS. The detailed methods of elemental analysis can be found in Srivastava et al (2020).

Enrichment factors (EFs) can be used to study the degree of elemental enrichment in ambient particles and can also help to determine whether they are from natural or anthropogenic emissions. The calculation of EFs are as follow,

$$EF=\frac{\left(C_x/C_{Al}\right)_{PM_{2.5}}}{\left(C_x/C_{Al}\right)_{Soil}}$$

Where, $\left(C_x/C_{Al}\right)_{PM_{2.5}}$ is the concentration ratio of x to Al in the measured $PM_{2.5}$ samples, $\left(C_x/C_{Al}\right)_{Soil}$ is the concentration ratio of x to Al of fugitive dust in Chinese Loess Plateau (Cao et al., 2008), respectively. Here, Al is the reference element due to its stability and immunity to human interference (Uematsu et al., 1983; Zhang et al., 2003).

The EFs of Si, Fe and Ti are listed in Table 1 (shown as Table S5 in SI). EF(Si) is in the range of 0.41 to 1.07, indicating that Si is mostly from natural sources. EF(Fe) and EF(Ti) are in range of 0.02-10.82 and 0-6.38, respectively, indicating that Fe and Ti are from mixed sources. Thus, we used Si concentrations and the Si to OC ratio from the Chinese Loess Plateau (Cao et al., 2008) and from Beijing road dust samples (Hu et al., 2019) to calculate a possible range OC from dust (OC_{dt}). We also calculate OC from dust (OC_{dt-Al}) using Al concentrations and the Al to OC ratio for comparison. The ranges of OC_{dt} and OC_{dt-Al} are listed in Table 1. The OC_{dt} and OC_{dt-Al} would result in a contribution to OC of 0.1-22.8% and 0.2-22.1%, respectively. And the calculated OC_{dt} would contribute 1.9% to 192.5% of OC_{onf} for PG site. It implies the OC from dust may be a major contributor to the primary non-fossil sources at PG.

Our other research on source apportionment of $PM_{2.5}$ using PMF has presented a detailed study of dust contributions (Srivastava et al., 2020). It showed that the crustal dust made a significant contribution to OC and EC. But it cannot clearly be attributed to soil dust or road dust, and contains mixed characteristics. The estimated dust contributions in urban Beijing were 12.7% during haze periods ($PM_{2.5}$ > 75 µg m^{-3}) and 35.2% during non-haze periods ($PM_{2.5}$ < 75 µg m^{-3}). The huge discrepancy between the methods is not easily explained, but Srivastava et al. (2020) urge caution in accepting their results.

References

Bhattarai, H., Saikawa, E., Wan, X., Zhu, H., Ram, K., Gao, S., Kang, S., Zhang, Q., Zhang, Y., Wu, G., Wang, X., Kawamura, K., Fu, P., and Cong, Z.: Levoglucosan as a tracer of biomass burning: Recent progress and perspectives, Atmos. Res., 220, https://doi.org/10.1016/j.atmosres.2019.01.004 20-33, 2019.

Cao, J. J., Chow, J. C., Watson, J. G., Wu, F., Han, Y. M., Jin, Z. D., Shen, Z. X., and An, Z. S.: Size-differentiated source profiles for fugitive dust in the Chinese Loess Plateau, Atmos. Environ., 42, 2261-2275, https://doi.org/10.1016/j.atmosenv.2007.12.041, 2008.

Dhammapala, R., Claiborn, C., Jimenez, J., Corkill, J., Gullett, B., Simpson, C., and Paulsen, M.: Emission factors of PAHs, methoxyphenols, levoglucosan, elemental carbon and organic carbon from simulated wheat and Kentucky bluegrass stubble burns, Atmos. Environ., 41, 2660-2669, https://doi.org/10.1016/j.atmosenv.2006.11.023, 2007.

Fine, P. M., Cass, G. R., and Simoneit, B. R. T.: Chemical characterization of fine particle emissions from fireplace combustion of woods grown in the northeastern United States, Environ. Sci. Technol., 35, 2665-2675, https://doi.org/10.1021/es001466k, 2001.

Fine, P. M., Cass, G. R. and Simoneit, B. R. T.: Chemical characterization of fine particle emissions from the fireplace combustion of woods grown in the southern United States, Environ. Sci. Technol., 36, 1442-1451, https://doi.org/10.1021/es0108988, 2002.

Fine, P. M., Cass, G. R., and Simoneit, B. R. T.: Chemical characterization of fine particle emissions from the wood stove combustion of prevalent United States tree species, Environ. Eng. Sci., 21, 705-721, https://doi.org/10.1089/ees.2004.21.705, 2004.

Fushimi, A., Saitoh, K., Hayashi, K., Ono, K., Fujitani, Y., Villalobos, A. M., Shelton, B. R., Takami, A., Tanabe, K. & Schauer, J. J.: Chemical characterization and oxidative potential of particles emitted from open burning of cereal straws and rice husk under flaming and smoldering conditions, Atmos. Environ., 163, 118-127, https://doi.org/10.1016/j.atmosenv.2017.05.037, 2017.

Gonçalves, C., Alves, C., Evtyugina, M., Mirante, F., Pio, C., Caseiro, A., Schmidl, C., Bauer, H., and Carvalho, F.: Characterisation of PM_{10} emissions from woodstove combustion of common woods grown in Portugal, Atmos. Environ., 44, 4474-4480, https://doi.org/10.1016/j.atmosenv.2010.07.026, 2010.

Hays, M. D., Geron, C. D., Linna, K. J., Smith, N. D., and Schauer, J. J.: Speciation of gas-phase and fine particle emissions from burning of foliar fuels, Environ. Sci. Technol., 36, 2281-2295, https://doi.org/10.1021/es0111683, 2002.

Hays, M. D., Fine, P. M., Geron, C. D., Kleeman, M. J., and Gullett, B. K.: Open burning of agricultural biomass: Physical and chemical properties of particle-phase emissions, Atmos. Environ., 39, 6747-6764, https://doi.org/10.1016/j.atmosenv.2005.07.072, 2005.

Hu, Y., Li, M., Yan, X., Zhang, C.: Characteristics and Interannual Variation of Chemical Components in Typical Road Dust in Beijing. Environmental Science, 40, 1645-1655, https://doi.org/10.13227/j.hjkx.201808224, 2019.

Liu, J., Li, J., Zhang, Y., Liu, D., Ding, P., Shen, C., Shen, K., He, Q., Ding, X., Wang, X., Chen, D., Szidat, S., and Zhang, G.: Source Apportionment Using Radiocarbon and Organic Tracers for PM2.5 Carbonaceous Aerosols in Guangzhou, South China: Contrasting Local- and Regional-Scale Haze Events, Environ. Sci. Technol., 48, 12002-12011, 10.1021/es503102w, 2014.

Mazzoleni, L. R., Zielinska, B., and Moosmüller, H.: Emissions of levoglucosan, methoxy phenols, and organic acids from prescribed burns, laboratory combustion of wildland fuels, and residential wood combustion, Environ. Sci. Technol., 41, 2115-2122, https://doi.org/10.1021/es061702c, 2007.

Ni, H. Y., Huang, R.-J., Cao, J. J., Liu, W. G., Zhang, T., Wang, M., Meijer, H. A. J., and Dusek, U.: Source apportionment of carbonaceous aerosols in Xi'an, China: insights from a full year of measurements of radiocarbon and the stable isotope ^{13}C, Atmos. Chem. Phys., 18, 16,363-16,383, https://doi.org/10.5194/acp-18-16363-2018, 2018.

Ni, H. Y., Huang, R. J., Cao, J. J., Dai, W. T., Zhou, J. M., Deng, H. Y., Aerts-Bijma, A., Meijer, H. A. J., and Dusek, U.: High contributions of fossil sources to more volatile organic aerosol, Atmospheric Chemistry and Physics, 19, 10405-10422, 10.5194/acp-19-10405-2019, 2019.

Sang-Arlt, X., Fu, H. X., Zhang, Y. A., Ding, X., Wang, X. M., Zhou, Y. N., Zou, L. L., Zellmer, G. F., and Engling, G.: Carbonaceous aerosol emitted from biofuel household stove combustion in South China, Atmosphere, 11, 112, https://doi.org/10.3390/atmos11010112, 2020.

Schauer, J. J., Kleeman, M. J., Cass, G. R., and Simoneit, B. R. T.: Measurement of emissions from air pollution sources. 3. C_1-C_{29} organic compounds from fireplace combustion of wood, Environ. Sci. Technol., 35, 1716-1728, https://doi.org/10.1021/es001331e, 2001.

Schmidl, C., Bauer, H., Dattler, A., Hitzenberger, R., Weissenboeck, G., Marr, I. L., and Puxbaum, H.: Chemical characterisation of particle emissions from burning leaves, Atmos. Environ., 42, 9070-9079, https://doi.org/10.1016/j.atmosenv.2008.09.010, 2008a.

Schmidl, C., Marr, L. L., Caseiro, A., Kotianová, P., Berner, A., Bauer, H., Kasper-Giebl, A., and Puxbaum, H.: Chemical characterisation of fine particle emissions from wood stove combustion of common woods growing in mid-European Alpine regions, Atmos. Environ., 42, 126-141, https://doi.org/10.1016/j.atmosenv.2007.09.028, 2008b.

Srivastava, D., Xu, J., Vu, T. V., Liu, D., Li, L., Fu, P., Hou, S., Shi, Z., Harrison, R. M.: Insight into PM2.5 sources by applying Positive Matrix factorization (PMF) at an urban and rural site of Beijing, (in review), 2020.

Sun, J., Shen, Z. X., Zhang, Y., Zhang, Q., Lei, Y. L., Huang, Y., Niu, X. Y., Xu, H. M., Cao, J. J., Ho, S. S. H., and Li, X. X.: Characterization of $PM_{2.5}$ source profiles from typical biomass burning of maize straw, wheat straw, wood branch, and their processed products (briquette and charcoal) in China, Atmos. Environ., 205, 36-45, https://doi.org/10.1016/j.atmosenv.2019.02.038, 2019.

Uematsu, M., Duce, R. A., Prospero, J. M., Chen, L., Merrill, J. T., and McDonald, R. L.: Transport of mineral aerosol from Asia Over the North Pacific Ocean, Journal of Geophysical Research: Oceans, 88, 5343-5352, https://doi.org/10.1029/JC088iC09p05343, 1983.

Xu, J., Srivastava, D., Wu, X., Hou, S., Vu, Tuan V., Liu, D., Sun, Y., Vlachou, A., Moschos, V., Salazar, G., Szidat, S., Prévôt, A. S. H., Fu, P., Harrison, R. M., and Shi, Z.: An evaluation of source apportionment of fine OC and PM2.5 by multiple methods: APHH-Beijing campaigns as a case study, Faraday Discussions, https://doi.org/10.1039/D0FD00095G, 2021.

Wang, Z., Bi, X., Sheng, G., and Fu, J.: Characterization of organic compounds and molecular tracers from biomass burning smoke in South China I: Broad-leaf trees and shrubs, Atmos. Environ., 43, 3096-3102, https://doi.org/10.1016/j.atmosenv.2009.03.012, 2009.

Yan, C., Zheng, M., Sullivan, A. P., Shen, G., Chen, Y., Wang, S., Zhao, B., Cai, S., Desyaterik, Y., Li, X., Zhou, T., Gustafsson, Ö., and Collett, Jr. J. L.: Residential coal combustion as a source of levoglucosan in China, Environ. Sci. Technol., 52, 1665-1674, https://doi.org/10.1021/acs.est.7b05858, 2018.

Zhang, X. Y., Gong, S. L., Shen, Z. X., Mei, F. M., Xi, X. X., Liu, L. C., Zhou, Z. J., Wang, D., Wang, Y. Q., and Cheng, Y.: Characterization of soil dust aerosol in China and its transport and distribution during 2001 ACE-Asia: 1. Network observations, Journal of Geophysical Research: Atmospheres, 108, https://doi.org/10.1029/2002JD002632, 2003.

Zhang, X., Lu, Y., Wang, Q. G., and Qian, X.: A high-resolution inventory of air pollutant emissions from crop residue burning in China, Atmos. Environ., 213, 207-214, https://doi.org/10.1016/j.atmosenv.2019.06.009, 2019.

Zhang, Y. L., Perron, N., Ciobanu, V. G., Zotter, P., Minguillón, M. C., Wacker, L., Prévôt, A. S. H., Baltensperger, U., and Szidat, S.: On the isolation of OC and EC and the optimal strategy of radiocarbon-based source apportionment of carbonaceous aerosols, Atmos. Chem. Phys, 12, 10,841-10,856, https://doi.org/10.5194/acp-12-10841-2012, 2012.

Zhang, Y.-X., Shao, M., Zhang, Y.-H., Zeng, L.-M., He, L.-Y., Zhu, B., Wei, Y.-J., and Zhu, X.-L.: Source profiles of particulate organic matters emitted from cereal straw burnings, J. Environ. Sci., 19, 167-175, https://doi.org/10.1016/S1001-0742(07)60027-8, 2007.

Zhao, X. Y., Hu, Q. H., Wang, X. M., Ding, X., He, Q. F., Zhang, Z., Shen, R. Q., Lu, S. J., Liu, T. Y., Fu, X. X., and Chen, L. G.: Composition profiles of organic aerosols from Chinese residential cooking: case study in urban Guangzhou, south China, Journal of Atmospheric Chemistry, 72, 1-18, 10.1007/s10874-015-9298-0, 2015.

Zhou, Y., Xing, X., Lang, J., Chen, D., Cheng, S., Wei, L., Wei, X., and Liu, C.: A comprehensive biomass burning emission inventory with high spatial and temporal resolution in China, Atmos. Chem. Phys., 17, 2839-2864, https://doi.org/10.5194/acp-17-2839-2017, 2017.

Table S1. Pearson correlations of species at IAP and PG sites.

IAP winter	$PM_{2.5}$	OC	EC	K^+	LG	MN	GA
$PM_{2.5}$	1.00						
OC	0.91	1.00					
EC	0.86	0.92	1.00				
K^+	0.74	0.67	0.71	1.00			
LG	0.56	0.60	0.74	0.51	1.00		
MN	0.52	0.57	0.72	0.48	0.99	1.00	
GA	0.52	0.55	0.70	0.52	0.98	0.97	1.00
PG winter	$PM_{2.5}$	OC	EC	K^+	LG	MN	GA
$PM_{2.5}$	1.00						
OC	0.95	1.00					
EC	0.85	0.93	1.00				
K^+	0.88	0.78	0.70	1.00			
LG	0.89	0.89	0.81	0.86	1.00		
MN	0.85	0.85	0.82	0.84	0.94	1.00	
GA	0.88	0.85	0.74	0.84	0.95	0.94	1.00
IAP summer	$PM_{2.5}$	OC	EC	K^+	LG	MN	GA
$PM_{2.5}$	1.00						
OC	0.72	1.00					
EC	0.34	0.79	1.00				
K+	0.65	0.64	0.36	1.00			
LG	0.52	0.59	0.36	0.85	1.00		
MN	0.47	0.55	0.37	0.80	0.97	1.00	
GA	0.41	0.59	0.54	0.59	0.79	0.85	1.00
PG summer	$PM_{2.5}$	OC	EC	K^+	LG	MN	GA
$PM_{2.5}$	1.00						
OC	0.60	1.00					
EC	0.41	0.75	1.00				
K+	0.65	0.80	0.57	1.00			
LG	0.42	0.46	0.32	0.51	1.00		
MN	0.47	0.22	-0.03	0.17	0.65	1.00	
GA	0.53	0.30	0.03	0.22	0.33	0.55	1.00

LG, MN and GA referred to levoglucosan, mannosan and galactosan, respectively.

Table S2. Summary of fire spot intensity, transport direction and sources of biomass burning.

Site	Date	$PM_{2.5}$ µg m^{-3}	EC_{nf} µg m^{-3}	LG ng m^{-3}	Fire spots intensity	Transport	Sources of biomass burning
IAP	2016/11/22	10.9	0.14	96.1	Low	from IM and HB	Low intensity
IAP	2016/11/24	117.1	1.35	458.7	Low	from IM and HB	Local
IAP	2016/11/26	209.4	1.43	227.4	High	from IM and HB	Regional
IAP	2016/12/1	49.4	0.82	192.3	High	from IM and HB	Regional
IAP	2016/12/2	98.6	1.51	515.4	High	from IM and HB	Regional + local
IAP	2016/12/3	239.9	1.94	634.8	Low	from HB and SX	local
IAP	2016/12/4	128.6	1.02	321.7	Low	from IM and HB	local
PG	2016/11/22	16.8	0.85	216.6	Low	from IM and HB	Local
PG	2016/11/24	106.8	2.52	915.6	Low	from IM and HB	Local
PG	2016/11/26	239.6	4.34	913.7	High	from IM and HB	Regional + local
PG	2016/12/1	41.0	1.22	311.2	High	from IM and HB	Regional
PG	2016/12/2	138.2	1.34	780.0	High	from IM and HB	Regional + local
PG	2016/12/3	281.5	2.62	1406.3	Low	from HB and SX	Strong local
PG	2016/12/4	294.3	2.70	1796.1	Low	from IM and HB	Strong local
IAP	2017/5/24	12.2	0.55	13.0	High	from IM, LN, HB	Regional
IAP	2017/5/26	34.7	0.44	22.1	High	from IM, HB	Regional
IAP	2017/5/27	78.8	0.49	20.1	High	from IM, HB	Regional
IAP	2017/6/10	18.6	0.46	11.6	Low	from IM, LN, HB	Low intensity
IAP	2017/6/16	44.3	0.40	51.9	High	from SD, HB	Regional + local
IAP	2017/6/17	66.7	0.77	179.6	High	from SX, HB	Regional + local
PG	2017/5/26	37.4	0.58	56.4	High	from SD, HB	Regional
PG	2017/5/27	70.3	0.85	89.8	High	from IM, HB	Regional + local
PG	2017/6/10	11.6	0.65	56.9	Low	from HB, TJ	Local
PG	2017/6/16	47.4	0.72	107.1	Very high	from HB	Regional + local
PG	2017/6/17	46.7	0.96	219.8	Very high	from IM, SX, HB	Regional + local

IM: Inner Mongolia, HB: Hebei, SD: Shandong, SX: Shanxi, TJ: Tianjin

Table S3. Summary of EC/OC and OC/LG ratios of different biomass types and the ranges of fractions in LG.

No.	Sample	EC/OC	OC/LG	Reference
1	Slash pine	0.141	0.341	Fine et al., 2002
2	Ponderosa pine	0.014	7.83	Fine et al., 2001
3	Western hemlock	0.050	2.52	Hays et al., 2002
4	Loblolly pine	0.178	1.02	Fine et al., 2002
5	Douglas fir	0.098	2.45	Fine et al., 2004
6	Eastern hemlock	0.053	10.5	Fine et al., 2001
7	White pine needle	0.078	7.18	Mazzoleni et al., 2007
8	Larch	0.176	3.68	Schmidl et al., 2008b
9	Balsam fir	0.066	12.3	Fine et al., 2001
10	Douglas fir (catalyst)	0.338	2.52	Fine et al., 2004
11	Loblolly pine	0.307	3.95	Fine et al., 2004
12	Chestnut oak	0.312	3.94	Wang et al., 2009
13	White pine needle	0.282	4.71	Mazzoleni et al., 2007
14	White pine needle	0.242	6.61	Mazzoleni et al., 2007
15	Spruce	0.384	5.02	Schmidl et al., 2008b
16	Mixed wood	0.288	6.76	Mazzoleni et al., 2007
17	White pine needle	0.331	6.64	Mazzoleni et al., 2007
18	Chinese evergreen Chinkapin	0.078	33.8	Wang et al., 2009
19	Chinese red pine	0.375	8.33	Sang-Arlt et al., 2020
20	Cape jasmine	0.137	27.9	Wang et al., 2009
21	Ponderosa pine needles	0.401	10.2	Mazzoleni et al., 2007
22	Common aporusa	0.095	43.3	Wang et al., 2009
23	Samak	0.054	137	Wang et al., 2009
24	Cedar wood	0.090	96.9	Mazzoleni et al., 2007
25	Excelsior	1.080	5.87	Mazzoleni et al., 2007
26	Excelsior	1.090	6.13	Mazzoleni et al., 2007
27	Eastern white pine	0.426	19.1	Fine et al., 2001
28	Maritime pine	1.420	6.87	Goncalves et al., 2010

29	China fir	0.651	16.7	Sang-Arlt et al., 2020
30	Ponderosa pine needles	1.320	15.4	Mazzoleni et al., 2007
31	Cedar wood	0.264	94.4	Mazzoleni et al., 2007
32	Ponderosa pine needles	1.500	17.4	Mazzoleni et al., 2007
33	Wood	0.500	55.6	Schmidl et al., 2008a
34	Ponderosa pine needles	0.632	55.4	Mazzoleni et al., 2007
35	Tamarak pine wood	0.330	137	Mazzoleni et al., 2007
36	Ponderosa pine sticks	3.320	20.1	Mazzoleni et al., 2007
37	Ponderosa pine sticks	3.680	25.6	Mazzoleni et al., 2007
38	Wood branch charcoal	0.393	625	Sun et al., 2019
39	Spruce with green needles	0.401	2128	Schmidl et al., 2008b
40	Pine	0.508	2128	Schauer et al., 2001
41	Pine with green needles	0.600	3571	Schauer et al., 2001
No.	Sample	EC/OC	OC/LG	Reference
42	Wheat straw	0.223	4.07	Sun et al., 2019
43	Wheat straw	0.068	15.4	Fushimi et al., 2017
44	Wheat straw	0.083	15.2	Fushimi et al., 2017
45	Wheat straw	0.184	12.5	Dhammapala et al., 2007
46	Wheat straw	0.422	10	Hays et al., 2005
47	Wheat straw	0.510	9.09	Mazzoleni et al., 2007
48	Maize straw	0.257	3.18	Sun et al., 2019
49	Maize straw	0.106	55.6	Yan et al., 2018
50	Cereal straw	0.130	12	Zhang et al., 2007

Table S4. The estimated OC/$EC_{nf, min}$ and OC/$EC_{f, min}$ ratios for IAP and PG sites during the whole winter and summer sampling period

	lowest 5 % OC/EC	lowest 2 $\frac{f_{NF,OC}}{f_{NF,EC}}$	lowest 2 $\left(\frac{1-f_{NF,OC}}{1-f_{NF,EC}}\right)$	Estimated OC/$EC_{nf, min}$	Estimated OC/$EC_{f, min}$
IAP winter	4.35	0.70	0.96	3.06	4.16
PG winter	6.27	0.76	0.81	4.76	5.09
IAP summer	4.65	0.73	0.78	3.41	3.62
PG summer	4.45	0.88	0.62	3.92	2.76

$f_{NF, OC}$ and $f_{NF, EC}$ are the non-fossil fractions of OC and EC, (1- $f_{NF, OC}$) and (1- $f_{NF, EC}$) are the fossil fractions of OC and EC.

Table S5. Summary of Cholesterol and element concentrations, EFs, $OC_{ck\text{-}ch}$, OC_{onf}, OC_{dt} and $OC_{dt\text{-}Al}$.

Site	Date	Cholesterol ng m^{-3}	Si ng m^{-3}	Al ng m^{-3}	Fe ng m^{-3}	Ti ng m^{-3}	$OC_{ck\text{-}ch}$ µg m^{-3}	OC_{onf} µg m^{-3}	EF(Si)	EF(Fe)	EF (Ti)	OC_{dt} µg m^{-3}	$OC_{dt\text{-}Al}$ µg m^{-3}
IAP	22/11/2016	1.10	141.6	68.8	190.4	34.6	2.16	-2.23	0.71	2.64	6.38	0.02-0.14	0.03-0.15
IAP	24/11/2016	1.39	335.2	229.5	526.9	8.8	2.71	-1.80	0.50	2.19	0.49	0.05-0.32	0.10-0.50
IAP	26/11/2016	1.08	2819.5	1372.1	1053.1	68.8	2.11	-0.11	0.71	0.73	0.64	0.41-2.70	0.58-3.01
IAP	01/12/2016	1.61	459.7	313.7	350.7	0.0	3.15	-2.22	0.51	1.06	0.00	0.07-0.44	0.13-0.69
IAP	02/12/2016	0.18	778.7	569.8	435.8	3.1	0.36	0.62	0.47	0.73	0.07	0.11-0.75	0.24-1.25
IAP	03/12/2016	0.37	1551.3	1319.9	1032.8	25.6	0.72	1.17	0.41	0.75	0.25	0.22-1.49	0.55-2.90
IAP	04/12/2016	1.73	2244.7	1635.2	467.0	18.3	3.38	-2.34	0.47	0.27	0.14	0.33-2.15	0.69-3.59
IAP	24/05/2017	0.46	43.4	25.0	283.9	5.7	0.90	0.77	0.60	10.82	2.89	0.01-0.04	0.01-0.05
IAP	26/05/2017	1.14	645.2	297.3	621.8	27.6	2.22	-1.05	0.75	1.99	1.18	0.09-0.62	0.12-0.65
IAP	27/05/2017	1.65	741.6	346.6	1149.8	32.1	3.22	-1.83	0.74	3.16	1.17	0.11-0.71	0.15-0.76
IAP	10/06/2017	0.38	1102.6	466.2	579.6	32.7	0.73	0.64	0.82	1.18	0.89	0.16-1.06	0.20-1.02
IAP	16/06/2017	0.40	793.0	302.9	433.0	37.3	0.78	-0.05	0.90	1.36	1.56	0.11-0.76	0.13-0.67
IAP	17/06/2017	1.00	584.0	188.2	488.7	19.9	1.96	-1.44	1.07	2.47	1.34	0.08-0.56	0.08-0.41
PG	22/11/2016	0.70	n.a	55.8	220.2	18.9	1.36	1.14	n.a	3.76	4.30	n.a	0.02-0.12
PG	24/11/2016	1.25	n.a	395.8	1354.9	51.9	2.44	4.31	n.a	3.26	1.66	n.a	0.17-0.87
PG	26/11/2016	1.75	n.a	1153.9	1979.3	164.7	3.42	9.65	n.a	1.63	1.81	n.a	0.48-2.53
PG	01/12/2016	1.08	n.a	111.2	244.5	2.6	2.11	1.45	n.a	2.09	0.30	n.a	0.05-0.24
PG	02/12/2016	0.94	n.a	452.6	625.0	5.6	1.84	1.03	n.a	1.32	0.16	n.a	0.19-0.99
PG	03/12/2016	1.46	n.a	897.2	1206.4	32.5	2.85	3.17	n.a	1.28	0.46	n.a	0.38-1.97
PG	04/12/2016	2.30	n.a	322.1	381.3	7.0	4.50	1.14	n.a	1.13	0.28	n.a	0.14-0.71
PG	26/05/2017	0.31	480.0	273.3	9.5	29.4	0.60	0.47	0.61	0.03	1.36	0.07-0.46	0.11-0.60
PG	27/05/2017	0.17	736.9	338.0	17.5	29.2	0.34	1.87	0.75	0.05	1.10	0.11-0.71	0.14-0.74
PG	10/06/2017	0.65	614.9	257.1	4.9	24.7	1.26	0.31	0.82	0.02	1.22	0.09-0.59	0.11-0.56
PG	16/06/2017	0.68	786.8	325.3	9.2	27.2	1.32	5.92	0.83	0.03	1.06	0.11-0.75	0.14-0.71
PG	17/06/2017	0.55	674.3	217.7	10.9	23.3	1.07	0.57	1.07	0.05	1.36	0.10-0.65	0.09-0.48

Table S6. Correlations and slopes among WINSOC, WSOC, POC, SOC, OC_{bb} and OC_{ck} at IAP and PG in winter and summer.

x	y	IAP winter		PG winter		IAP summer		PG summer	
		slope	R^2	slope	R^2	slope	R^2	slope	R^2
POC_f	$WINSOC_f$	1.11	0.97	1.23	0.97	0.92	0.93	0.84	0.82
	$WSOC_f$	0.57	0.99	0.61	0.84	0.96	0.92	0.58	0.55
SOC_f	$WINSOC_f$	1.53	0.96	1.27	0.89	0.99	0.91	0.98	0.45
	$WSOC_f$	0.78	0.93	0.69	0.96	1.05	0.93	0.89	0.67
OC_{bb}	$WINSOC_{nf}$	1.59	1.00	2.38	0.94	1.16	0.44	1.58	0.91
	$WSOC_{nf}$	1.64	0.94	1.70	0.92	3.41	0.93	1.54	0.93
OC_{ck}	$WINSOC_{nf}$	3.54	0.88	1.68	0.69	1.08	0.74	2.26	0.27
	$WSOC_{nf}$	3.83	0.94	1.21	0.69	1.53	0.19	2.29	0.32
SOC_{nf}	$WINSOC_{nf}$	0.85	0.98	0.98	0.83	0.42	0.65	0.79	0.92
	$WSOC_{nf}$	0.90	0.99	0.71	0.83	1.09	0.97	0.75	0.88

f: fossil sources, nf: non-fossil sources, bb: biomass burning, ck: cooking. Concentrations of fossil and non-fossil sources of WINSOC and WSOC were from ^{14}C measurement. POC, SOC, OC_{bb} and OC_{ck} are from extended Gelencsér method.

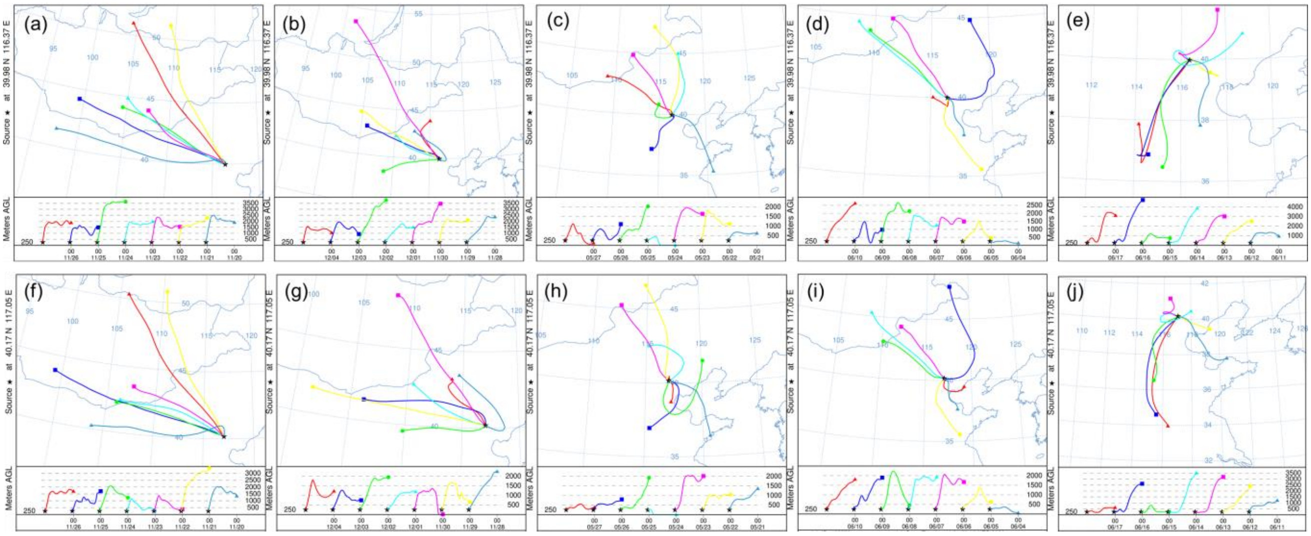

Figure S1. 48 h air-mass back trajectories with 24 h interval at 250 m, (a)-(e): destination at IAP, (f)-(j): destination at PG. (https://ready.arl.noaa.gov/HYSPLIT.php, last access: 12 June 2020)

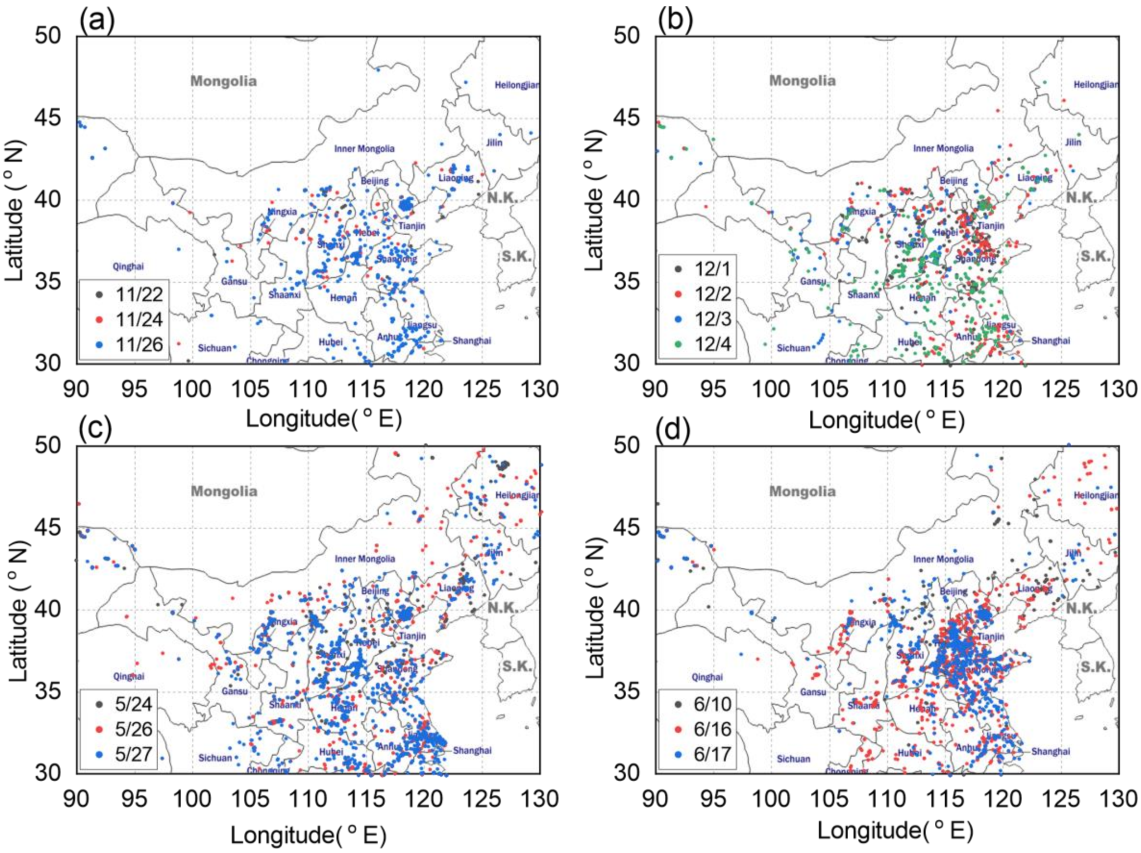

Figure S2. Fire spots observed by MODIS (AQUA/TERRA) (https://firms.modaps.eosdis.nasa.gov/alerts/, last access: 16 April 2020) around Beijing, coloured dots refer to fire spots on (a): 22, 24, 26 Nov 2016, (b): 1-4 Dec 2016, (c): 24, 26, 27 May 2017, (d) 10, 16, 17 Jun 2017.

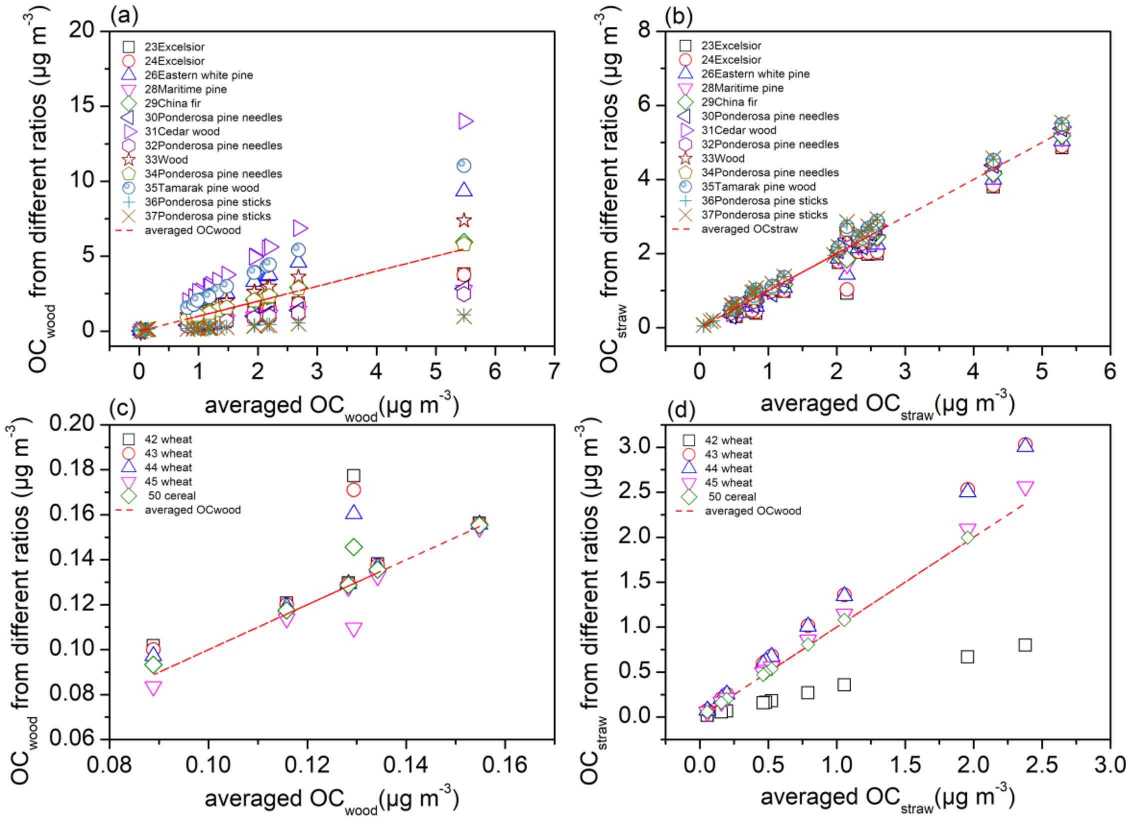

Figure S3. Correlations of averaged OC_{wood} with OC_{wood} from different ratios and averaged OC_{straw} with OC_{straw} from different ratios. (a), the influence of ratios from softwood on the estimation of OC_{wood}; (b), the influence of ratios from softwood on the estimation of OC_{straw}; (c), the influence of ratios from wheat straws on the estimation of OC_{wood}; (d), the influence of ratios from wheat straws on the estimation of OC_{straw}. As there is only one set of ratios from maize straw which matches the selection limitation, the influence of ratios from maize straw was not plotted. The legends correspond to the No. and types of samples in Table S3.

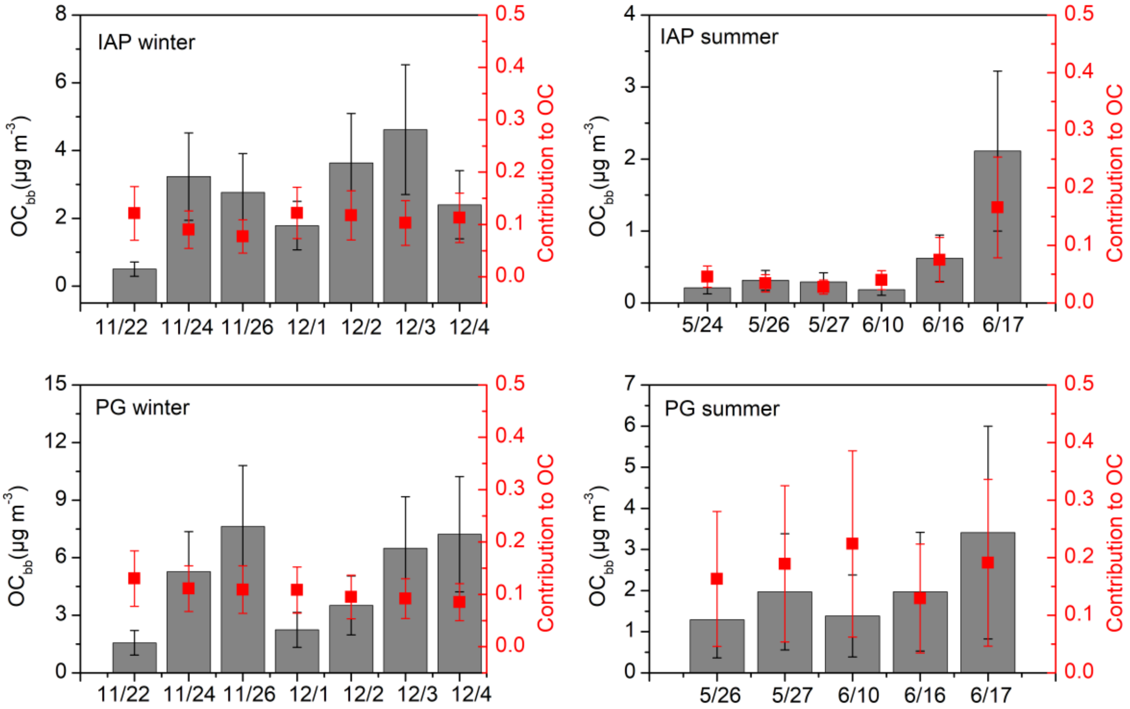

Figure S4. The mass concentrations and % contributions of OC_{bb} at IAP and PG during winter and summer.

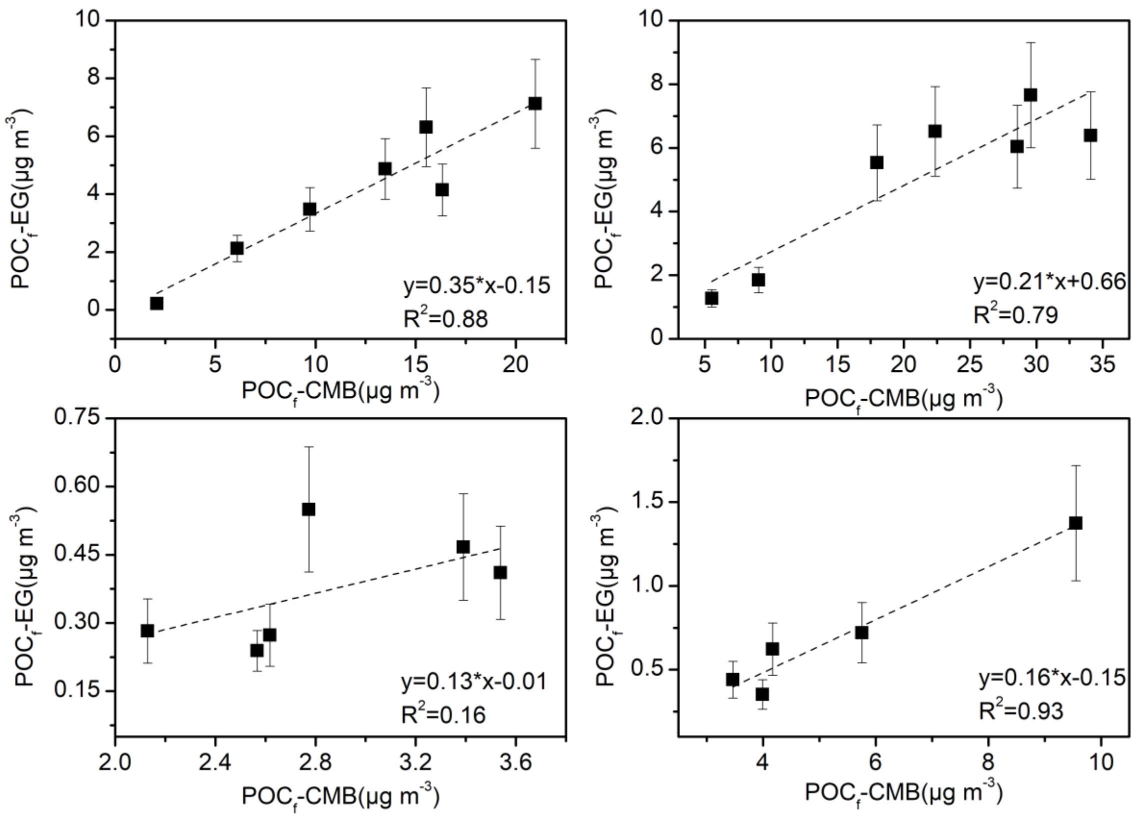

Figure S5. Correlations of POC_f from the extended Gelencsér method (POC_f-EG) and CMB if using $(POC/EC)_f$ ratios 1.12−2.08 in winter, 0.40−0.77 in summer.

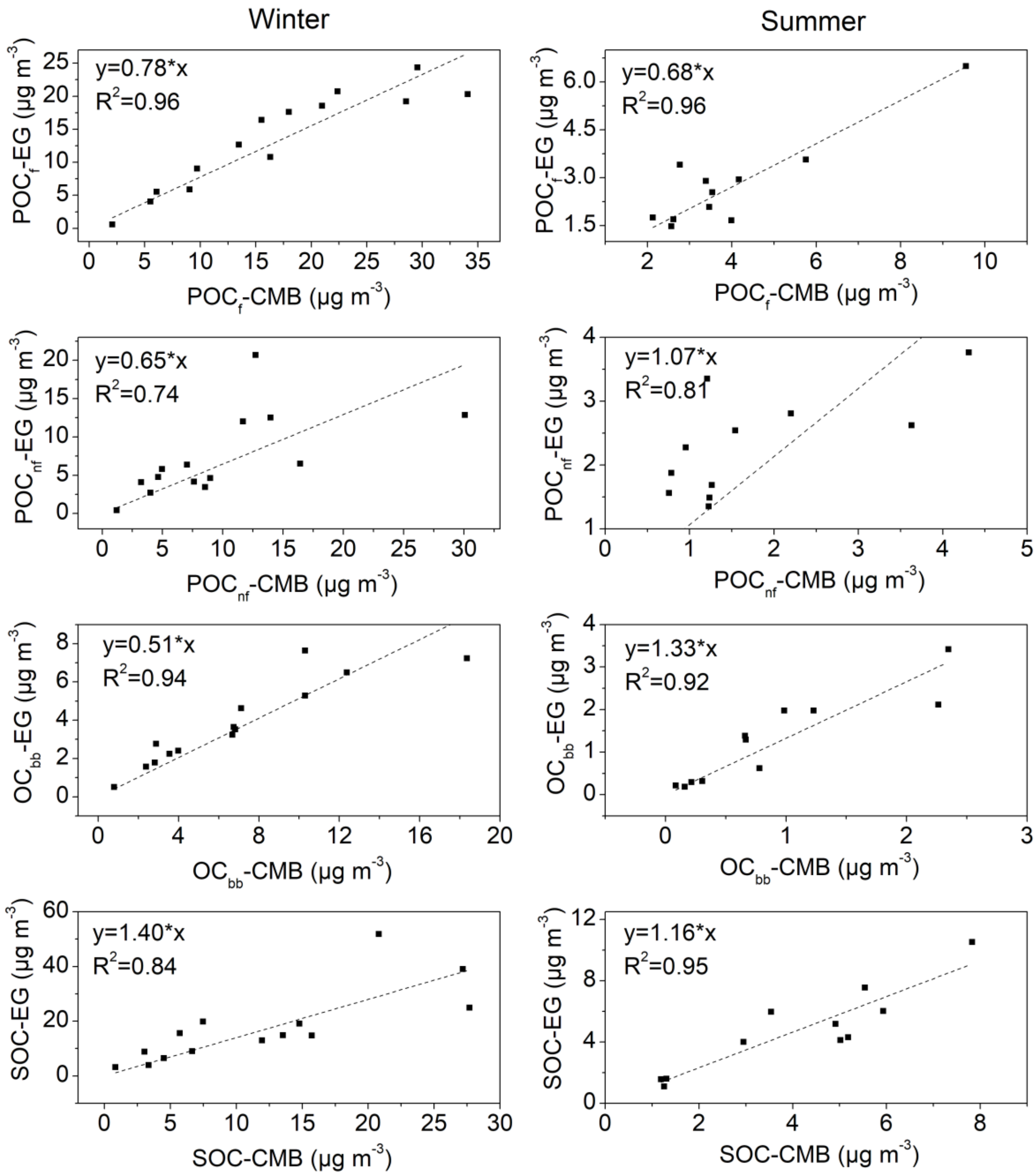

Figure S6. Correlations of OC sources from extended Gelencsér method with those from CMB model in winter (left) and summer (right). EG denotes extended Gelencsér method.

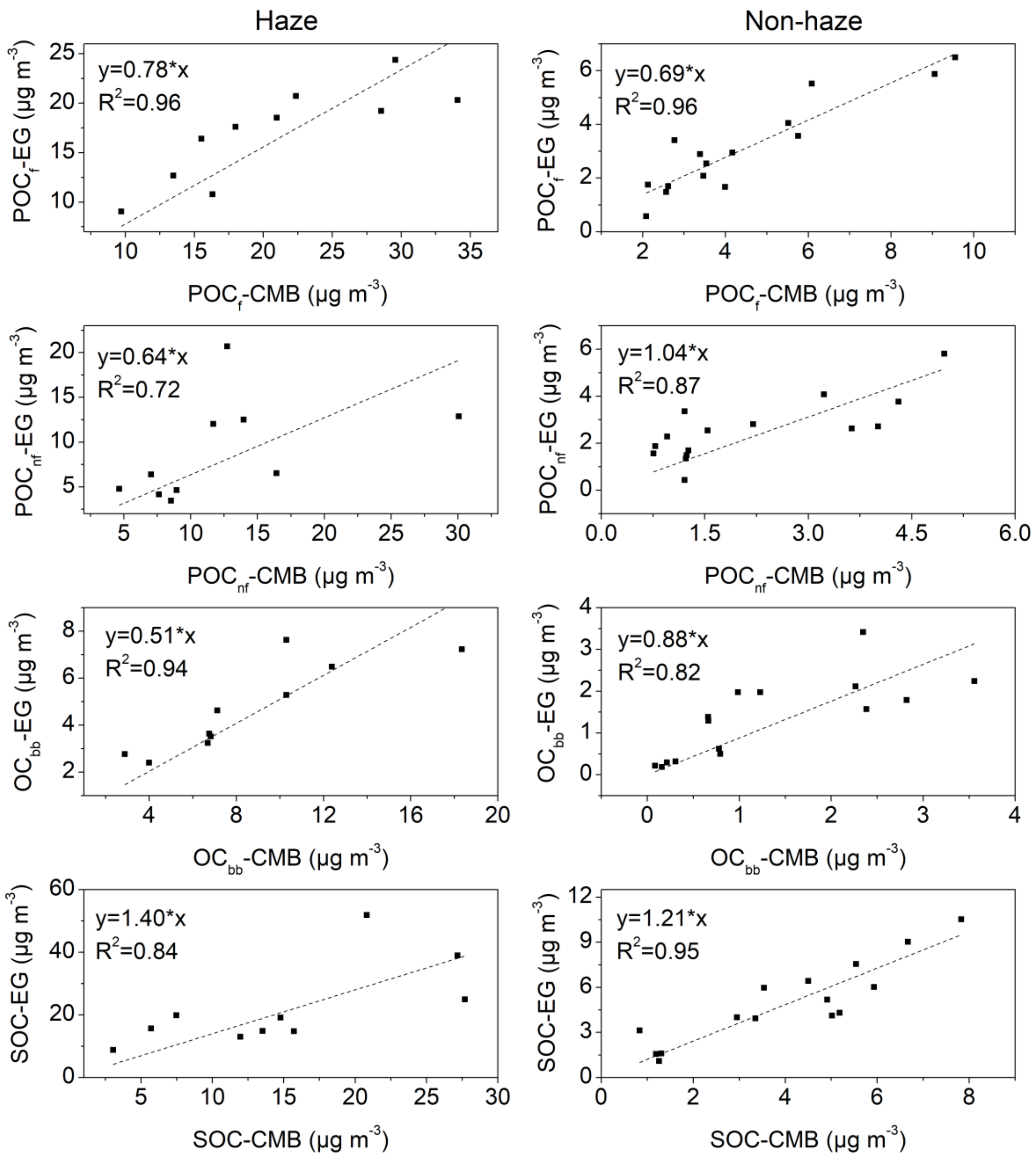

Figure S7. Correlations of OC sources from extended Gelencsér method with those from CMB model during haze period (left) and non-haze period (right). EG denotes extended Gelencsér method.

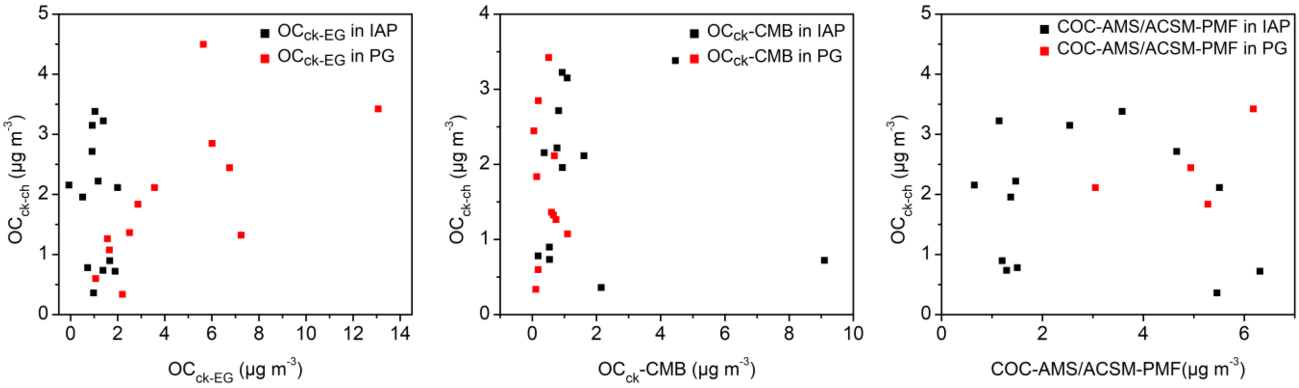

Figure S8. Correlations of $OC_{ck\text{-}ch}$ with $OC_{ck\text{-}EG}$, OC_{ck}-CMB and COC-AMS/ACSM-PMF. $OC_{ck\text{-}ch}$, OC from cooking from cholesterol concentrations and cholesterol to OC ratios; $OC_{ck\text{-}EG}$, OC from cooking from extended Gelencsér method; OC_{ck}-CMB, OC from cooking from CMB model; COC-AMS/ACSM-PMF, OC from cooking from AMS/ACSM-PMF model (AMS for IAP and ACSM for PG).

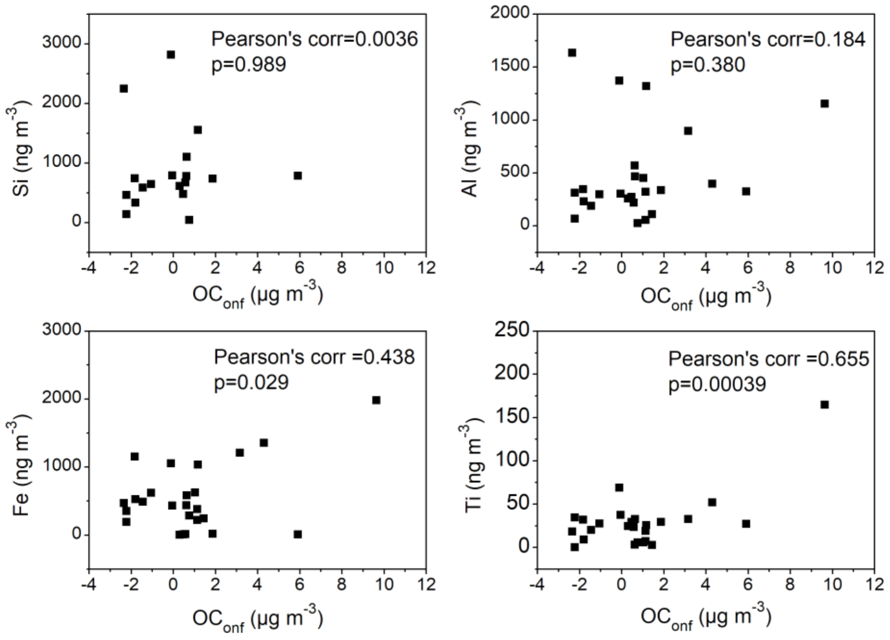

Figure S9. Correlations of OC_{onf} (=$OC_{ck\text{-}EG}$-$OC_{ck\text{-}ch}$) with Si (no data in winter campaign of PG), Al, Fe and Ti. $OC_{ck\text{-}ch}$, OC from cooking from cholesterol concentrations and cholesterol to OC ratios; $OC_{ck\text{-}EG}$, OC from cooking from extended Gelencsér method.